Simulation and Experimental Analysis of the Wind Field inside the Air Deflector of a Sugarcane Leaf Cutting and Returning to Field Machine

Zhenhua Xu[1, a]，Qianru Wang[2, b]， Yuxing Wang [1, c *], Feng Zhao[1]，Jiaxian Lu[1]

[1] Key Laboratory of Key Technology on Agricultural Machine and Equipment, Ministry of Education, South China Agricultural University, Guangzhou, 510642, China

[2] Department of Mechanical Engineering, Massachusetts Institute of Technology, Cambridge, Massachusetts, 02139, USA

[a] zhenhua090527@163.com，[b] qianru@mit.edu，[c] scauwyx@ scau.edu.cn,

Abstract: This work investigated the self-excited wind field caused by rotating knife rollers inside the air deflector during the operation of the sugarcane leaf cutting and returning to field machine. Based on the arbitrary Lagrangian-Eulerian (ALE) method, a fluid-structure interaction simulation of wind field inside the air deflector was carried out under the condition of two clockwise rotating knife rollers, exploiting the finite element software LS-DYNA. The simulation results revealed an airflow confluence surface generated during the process of the airflow interaction, accompanied by formation of vortices. The wind field in the left and right outlets of the air deflector and regions near the ground between the two knife rollers is regular and stable. Airflow velocities below the deflector near the ground were measured. With both simulation and experimental evidences, we demonstrate that the horizontal wind velocity decreases with an increasing elevation above the ground, with a simulation deviation of velocity decreasing rate no more than 12%. In contrast, the vertical wind velocity shows an opposite correlation with height, and the simulation deviation of velocity increasing rate is no more than 26%. Our simulation and experimental data indicate a consistent variation trend of wind velocity. Insights from this study can be useful in designing and optimization of relevant structures and mechanisms involving air deflectors and knife rollers.

1. Introduction

Most of the sugarcane-leaf-returning machines are equipped with rigid blades and driven by tractors. Although these machines have good performances in the process of returning sugarcane leaves to field, their overweight can cause soil compaction. Additionally, their rigid cutters damage the perennial roots of sugarcane easily. To address these issues, South China Agricultural University developed a sugarcane leaf returning to field machine with flexible nylon cutters and self-propelled caterpillar chassis. Experimental results showed that the wind field induced by the rotating flexible blades could blow away sugarcane leaves, leading to a reduced cutting efficiency. To solve this problem, a second generation prototype was established to mitigate the influence of wind field by adding an air deflector, using double knife rollers, and taking advantages of the hold down effect of the caterpillar chassis on the leaves [1-3]. It is crucial to have a thorough understanding of the wind field inside the air deflector and provide a theoretical basis for further optimizations of air deflector and knife roller. Since air is transparent and difficult to be experimentally visualized, finite element simulation was used to investigate the wind field induced by the rotating flexible blades inside the air deflector.

Based on finite element software LS-DYNA, the arbitrary Lagrangian-Eulerian (ALE) method has been widely applied to the fluid-structure interaction simulations of solid structure and air by researchers in China and abroad. Tutt et al. built the airflow model based on Eulerian algorithm and obtained the inflation characteristics of parachute through ALE algorithm [4-6]. Lingard et al. demonstrated the stimulation and analysis of parachute performance in supersonic flow, highlighting the numerical modeling of parachute and airflow and airflow mesh generation [7-8]. Jia He et al. and Cheng Han et al. studied the kinematics of parachute inflation process and

surrounding flow field, providing parameters of parachute and flow field variations during parachute inflation process [9-12]. Moreover, a number of studies were carried out to develop the fluid-structure interaction simulation of space vehicles landing process [13-14]. The finite element model of a manned spacecraft with parachute and the atmospheric environment involved was built using ALE method to simulate the interaction among the spacecraft, air and water during landing [15-16]. Cheng et al. established a water-structure-air model with ALE multi-material mesh considering both water, air missile, silo and cover plate by LS-DYNA. The process of sub-marine-launched missile without attack angle was simulated [17]. Based on the aforementioned works, we applied ALE method to analyze the wind field inside the air deflector of the sugarcane leaf cutting and returning to field machine using the finite element software LS-DYNA. The simulation results show the alteration trends of airflow inside the air deflector, which is consistent with the experimental results. Insights from this study will be useful in designing and optimization of structural and kinematic parameters.

2. Structure of the Sugarcane Leaf Cutting and Returning to Field Machine

The sugarcane leaf cutting and returning to field machine was equipped with a self-propelled caterpillar chassis and powered by batteries to provide walking and cutting operations. The air deflector and knife rollers were installed in the middle of the chassis. Two knife rollers were assembled on the sugarcane leaf cutting and returning to field machine, and each knife roller was equipped with two cutter disks, on which the flexible cutters made of nylon were installed (Fig.1). Power transmission between driving motor and knife rollers and between the two knife rollers was achieved through belt drive. During operations, the master knife roller was driven by the motor through the input belt, and the slave knife roller was driven by the master knife roller through the output belt, resulting in a high-speed rotation of the flexible nylon cutters to whip and cut the sugarcane leaves. The two knife rollers were shielded by the air deflector, while the driving motor, input and output belts and belt wheels were installed outside the air deflector. The self-excited wind field caused by the knife rollers was limited inside the air deflector, with the holding effect of the caterpillar chassis, preventing the sugarcane leaf debris from being blown away [2-3].
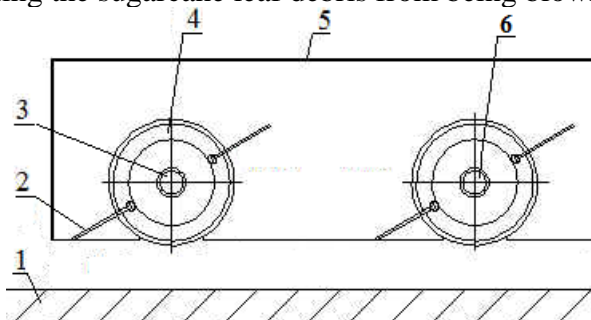
1. Ground 2.Nylon cutter 3.Master knife roller 4.Cutter disk 5.Air deflector 6.Slave knife roller
Fig.1 Structure sketch of knife roller and air deflector

3. Finite Element Model

3.1 Simulation Assumptions

(1) Neglect the moving displacement of sugarcane leaf cutting and returning to field machine, and assume it's static. The machine walking velocity is 0.3 m/s and the rotation speed of the knife rollers is 3,000 rpm, so the moving displacement of machine is insignificant during the process of cutting one piece of sugarcane leaf.

(2) Assume the ground is flat. The unevenness of sugarcane field was neglected to simplify the modeling.

(3) Given the small deformation, neglect the influence of deformation of ground, cutter disks and air deflector on wind field. Consider these three parts as rigid body to reduce operation time.

3.2 Modeling of Knife Roller, Air Deflector and Ground

The knife roller model consists of rotating shafts, cutter disks and nylon cutters. The modeling domain was limited to the structures inside the air deflector. The material model of the rotating shaft and cutter disk were set to the rigid material model MAT_RIGID, and the element type was solid 164. The density, elastic modulus and Poisson's ratio of rotating shaft and cutter disk was 7820 kg/m^3, 2.07×10^{11} Pa and 0.28, respectively.

The material of nylon cutter was PA66, whose density and shear modulus were 1,400 kg/m^3 and 3.01×109 Pa [18], respectively.

The element of air deflector was set as shell 163, and the shell element thickness was prescribed as 0.002 m in the real constant option. The material of air deflector was stainless steel, whose density, elastic modulus, and Poisson's ratio were 8,000 kg/m^3, 2.1×10^{11} Pa and 0.3, respectively.

The density, elastic modulus and Poisson's ratio of ground were 1,850 kg/m^3, 2.0×10^7 Pa and 0.3, respectively.

3.3 Air Model

Material model of the air was set to *MAT_NULL. Air density and dynamic viscosity were 1.25 kg/m^3 and 1.7456×10^{-5} Pa•s, respectively. Meanwhile, define the linear polynomial equation as *Eos _ Linear _ Polynomial. The gas state equation can be expressed as [16]:

$$P = C_0 + C_1\mu + C_2\mu^2 + C_3\mu^3 + \left(C_4 + C_5\mu + C_6\mu^2\right)e_{ipv0} \qquad (1)$$

Where $C_0 \sim C_6$ are constant coefficients of the linear polynomial equation. For ideal gas, there is usually an initial pressure. Since there are no direct input options available for the initial pressure in the state equation, it was inputted as $P_0 = C_0$, or through the transformed initial internal energy term expressed as:

$$P = (\gamma - 1)\frac{1}{\nu_{rel}}e_{ipv0} \qquad (2)$$

Where the gas heat capacity γ is 1.4, relative volume ν_{rel} is 1.0, and the pressure P is 101325 Pa, giving an initial internal energy $e_{ipv0} = 2.5331\times10^5$ J [19].

3.4 Model Building and Meshing

According to the actual size of the prototype, the simulation model was built in ANSYS Graphical User Interface directly with the m-kg-s unit system. The size of air domain is slightly bigger than that of the air deflector, and thus it covers the entire air deflector and knife rollers, as shown in Fig.2a. In order to reduce the grid scale and improve the calculation accuracy, the meshing of air domain was carefully optimized. The meshing elements in the vicinity of the nylon blade rotating area were refined, while the grid density of the remaining air domain was reduced. Additionally, in order to suppress the leakage problem, the mesh size of the air deflector was smaller than that of the air domain. The meshed model was shown in Fig.2b.
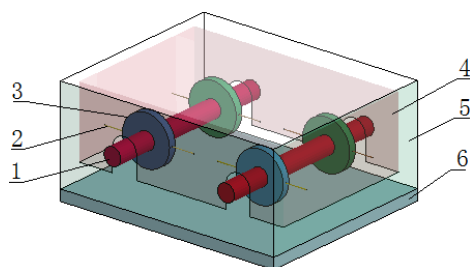
1. Rotating shaft 2. Flexible nylon cutter 3. Cutter disk
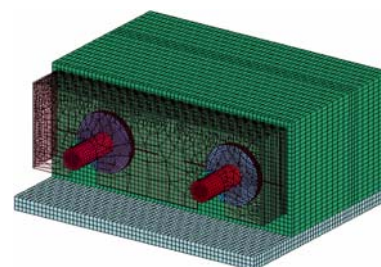4. Air deflector 5. Air 6. Ground
Fig.2a. unmeshed model

Fig.2b. Cutaway view of meshed model

Fig.2 Simulation model

3.5 Parameter Settings of Fluid-Structure Interaction

Some important parameters are not accessible in the ANSYS Graphical User Interface. After model

construction and meshing, the keywords file was exported from the ANSYS Graphical User Interface, and then was added with keywords for fluid-structure interaction control in LS-PrePost. The element type of air model was modified to *SECTION_SOLID_ALE. The keyword ALE *CONSTRAINED_LAGRANGE_IN_SOLID and *CONTROL_ALE were added into the keywords file. As to the settings of fluid-structure interaction keyword *CONSTRAINED_LAGRANAGE_IN_SOLID, set the air as MASTER, while the knife rollers, air deflector and ground as SLAVE, and choose the penalty function methods for coupling.

3.6 Loading the Rotation Velocity

Through rotation velocity measuring device, the rotation velocity of master knife roller was 3011 rpm, i.e. an angular velocity of 315.15 rad/s. The slave knife roller speed was 2876 rpm, i.e. an angular velocity of 300.08 rad/s. Both rollers were rotating clockwise. The prescriptions of the knife roller velocities and steering in the simulation were based on factual metering.

4. Simulation results and discussion

4.1 Analysis of wind field inside the air deflector

Within a 0.03 s time interval, the master knife roller and slave knife roller rotate clockwise for 180.6° and 172°, respectively. The airflow variations near the nylon rotating sections inside the air deflector at different instants are shown in Fig.3. In the region L (the area near the ground between two knife rollers, labeled by dashed box in Fig.3a), the airflow caused by the master knife roller moves in the lower-left direction (indicated by arrow d), while the airflow caused by the slave knife roller moves in the upper-left direction (arrow e). These two airflows converged in the area between two knife rollers. In region M (the area between two knife rollers near the ceiling of the air deflector), the airflow caused by the master knife roller moves towards the lower-right (arrow f), while the airflow caused by the slave knife roller moves to the upper-right (arrow g).

In Fig.3b, the nylon cutters of two knife rollers reach the vertical position. In region N, the airflow caused by the slave knife roller moves into the rotating region of the master knife roller. The downward movement of the nylon cutters on the master knife roller counteracts the airflow moving to the upper-left induced by the slave knife roller. As a result, the airflow is weakened gradually and changed to move in the lower-left direction (arrow h). In region O, under the influence of the upward movement of cutters on the slave knife roller, the lower-rightward airflow induced by the master knife roller is mitigated and changed to be upper-rightward (arrow i). Part of the airflows swirl and form vortices after the confluence (arrow j). Other airflows move to the right and gradually change to move in the horizontal direction under the effect of the air deflector.

In Fig.3c, the nylon cutters on the master knife roller rotate to a position close to horizontal. In region P (dashed box in Fig.3c), two airflows due to the master and slave knife rollers merge and exhaust from the left outlet of the air deflector (arrow k). Such a confluence of airflows is cyclic due to the rotation of two knife rollers.

a. Wind field，t=0.02s

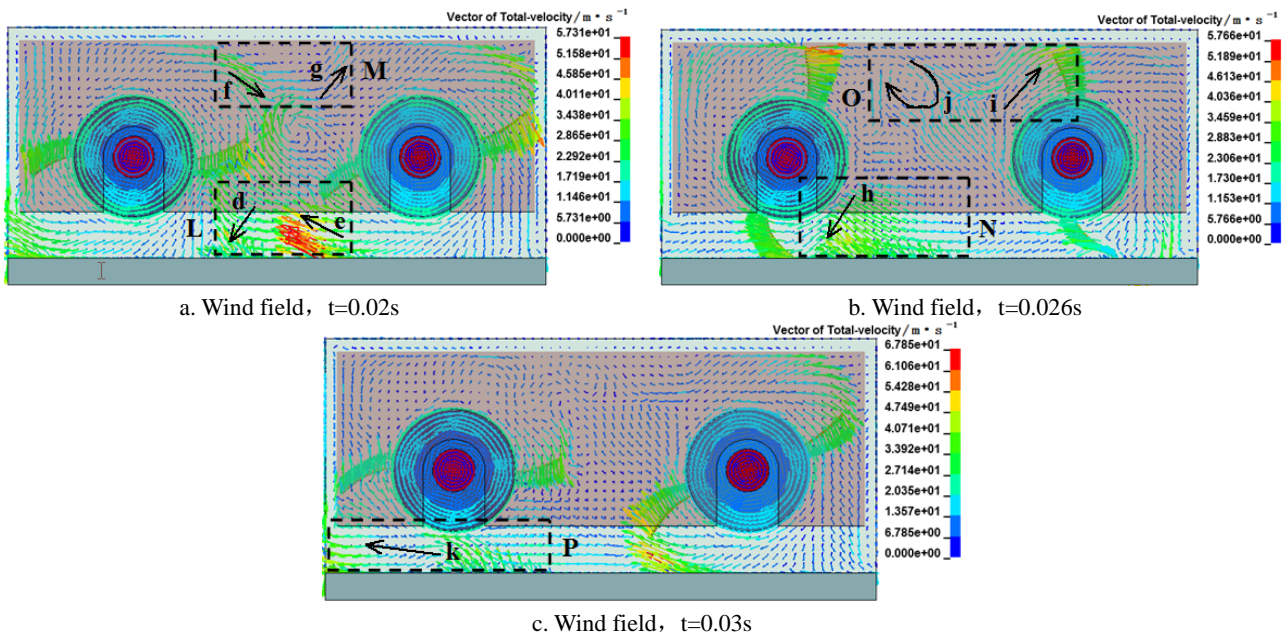

b. Wind field，t=0.026s

c. Wind field，t=0.03s

Fig.3 Movement of airflow inside the dome

Through the analysis of the simulation results, the interaction of two airflows caused by two knife rollers was obtained. An airflow confluence surface (Fig. 4) was generated in between these two knife rollers during the process of the airflow interaction, accompanied by the formation of one or two vortices. Due to the rotating velocity difference between the two knife rollers, the nylon cutters on the two knife rollers approach different positions after the third revolution. However, the airflow interaction process and the airflow confluence surface remained unchanged, as shown in Fig.4. Generally speaking, airflow near the ceiling of the air deflector moves to the right, while airflow near the ground moves to the left and escapes from the outlet of the air deflector.
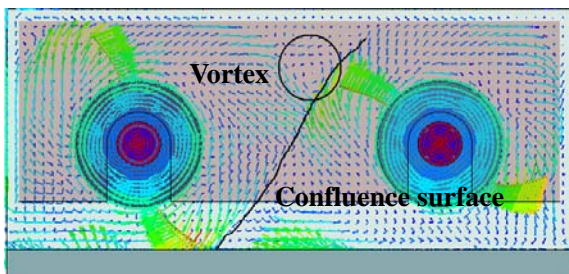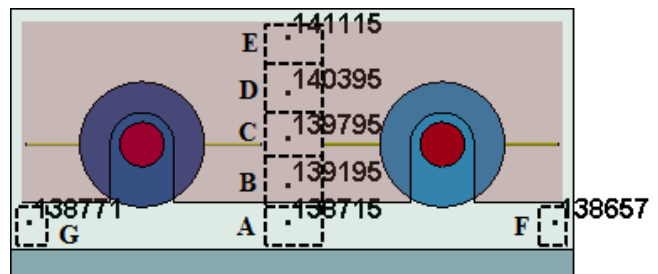

Fig.4 Airflow interaction area

Fig.5 Selected nodes

4.2 Analysis of Wind Velocity

Using the post-processing function of LS-PREPOST software, relevant data of airflows at various positions inside the air deflector was obtained. The airflow in the rotating plane of nylon cutters is the strongest. Airflow velocities, in the X (horizontal) and Y (vertical) directions, at a number of selected nodes (Fig. 5) are plotted.

In Fig.5, seven regions (region A to G) are selected, five of which are located between two knife rollers, at a vertical position of 0.03, 0.08, 0.13, 0.18 and 0.23 meter from the ground, numerated by 138715, 139195, 139795, 140395, and 141115, respectively. The other 2 nodes are located in the left and right outlets of the air deflector, both are 0.03 m above the ground, numerated by 138771 and 138657, respectively.

The airflow velocities of the selected nodes in X and Y directions are shown in Fig.6 and Fig.7. Before 0.04 s, activation of the knife rollers leads to sudden changes in airflow velocities in the air deflector, and the wind speed is high and unstable. With the continuous rotation of knife rollers, the

airflow inside the air deflector changes to a regular cyclic pattern. After 0.04s, the wind speed is stabilized within a frequency range between 50 and 100 Hz.
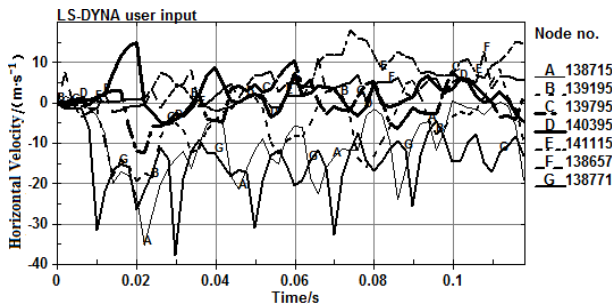

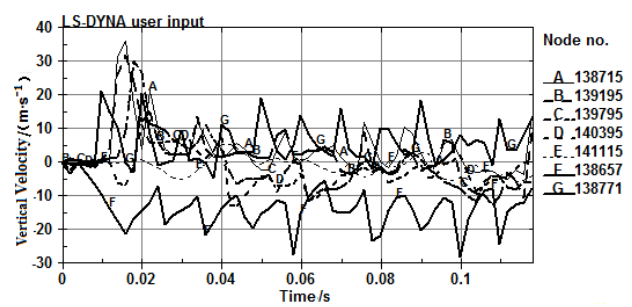Fig.6 Hodograph in horizontal direction of selected nodes

Fig.7 Hodograph in vertical direction of selected nodes

In terms of the horizontal wind speed, the airflow changes are more stable in the region G (the left outlet of the air deflector), the region A (the area near ground between two knife rollers) and the region F (the right outlet of the air deflector). By contrast, the airflow is fluctuating and left-right alternately directed in region B, C and D, corresponding to the middle area of the air deflector, because this area is in the confluence surface of the two airflows caused by two knife rollers. Overall, at the same elevation near the ground, wind velocities in region A, F and G follow a descending order as region G > region A > region F. The airflow in region F is rightward, while the airflow in region A and G is moving to the left. In the area between two knife rollers, corresponding to region ABCDE, the wind speed is decreasing with an increasing elevation.

On the other hand, the vertical wind speed has an abrupt increase before 0.04 s, and then turns into a regular fluctuation within a stable range after 0.04 s. The airflow alterations are consistent in region F and G. In region A, C and D, the airflow direction is stable, but no significant periodicity is observed in the variations of wind velocity. Additionally in region B and E, the airflow direction is alternating upward and downward. The wind velocity in region E is low and fluctuating around 0 m/s. In brief, at the same elevation near the ground, wind velocities in region A, F and G can be ordered degressively as region F > region G > region A. In the area between two knife rollers, corresponding to region ABCDE, the wind speed increases with an increasing elevation. However, such velocity increases in region B, C and D is trivial. .

Analysis of wind field and wind velocity in different regions inside the air deflector indicates that wind velocity variations are most regular and stable in regions near the ground between the two knife rollers, the around the left and right outlets of the air deflector. Most of the airflows near the ground move to the left and exhaust from the left outlet of air deflector. Moreover, inside the air deflector, the horizontal wind speed is high near the left outlet of the air deflector, moderate in between the two knife rollers near the ground, and low at the right outlet of the air deflector. Contrarily, the vertical wind speed at the right outlet of the air deflector is higher than that at the left outlet, which in turn is higher than the velocity near the ground between two knife rollers. Such a wind flow field is beneficial to the sugarcane leaves cutting. The sugarcane leaves are fed from the right outlet of the air deflector, pushed into the cutting area, and discharged from the left outlet of the air deflector. However, in the area between two knife rollers, the airflow moves to the upper-left direction, which can pull up the sugarcane leaves in the air. Moreover, the unstable airflow in the middle area of the air deflector can drive sugarcane leaves towards the knife rollers and cause intertwist problems. For future work, improvements can be achieved by adding a partition plate in the middle of the air deflector, in order to guide the airflows in the upper regions of the air deflector, avoid the formation of vortex, and stabilize airflows in these areas.

5. Comparison of simulation and experimental results

The comparative experiment was carried out to verify the simulation results. The wind velocity inside the air deflector was measured using a hot wire anemometer, with a 0.5 second data acquisition interval. Thus, the collected data represents a velocity averaged over 0.5 second.

In the experiment, because of the restriction of the car body frame and air deflector, only wind velocities in the regions below the air deflector were measured. Wind speeds were measured at three elevations, namely 0.01, 0.02 and 0.03 meters above the ground in the left and right outlets of the air deflector, and five elevations starting at 0.01 m above the ground with a 0.01 m increment in the area between two knife rollers. In order to measure the X and Y components of wind velocity, the probe was adjusted to the horizontal and vertical directions, respectively. Each condition was measured in triplicate within 25 to 30 seconds.

Simulation results at the nodes that match the measurement locations were compared with the corresponding experimental results. In Fig. 8, the simulation data is the averaged wind velocity after 0.04 s, while the experimental data is the velocity averaged over the testing time period. Both of the simulation and experimental results show that the horizontal wind velocity decreases with an increasing height. Overall, the horizontal wind velocity is the highest in the left outlet of the air deflector, moderate in the region between two knife rollers, and lowest near the right outlet of the air deflector, which is consistent with the simulation results. Comparison of the horizontal velocity decreasing rate derived from simulation and experiments gives a consistent velocity variation trend. Over a 0.01 to 0.03 m elevation difference above the ground, the simulated and experimental decreasing rates of horizontal wind velocity are 26% and 33% near the left outlet of the air deflector, 68% and 60% in the region between two knife rollers (where an elevation difference over 0.01 and 0.05 m was considered), and 17% and 29% near the right outlet of the air deflector, respectively. The maximum deviation of decreasing rate between the horizontal wind velocities obtained by simulation and experiments is 12%. Both the simulation and experimental data show a similar downtrend.

a. The left outlet of the air deflector   b.The area between two knife rollers   c. The right outlet of the air deflector
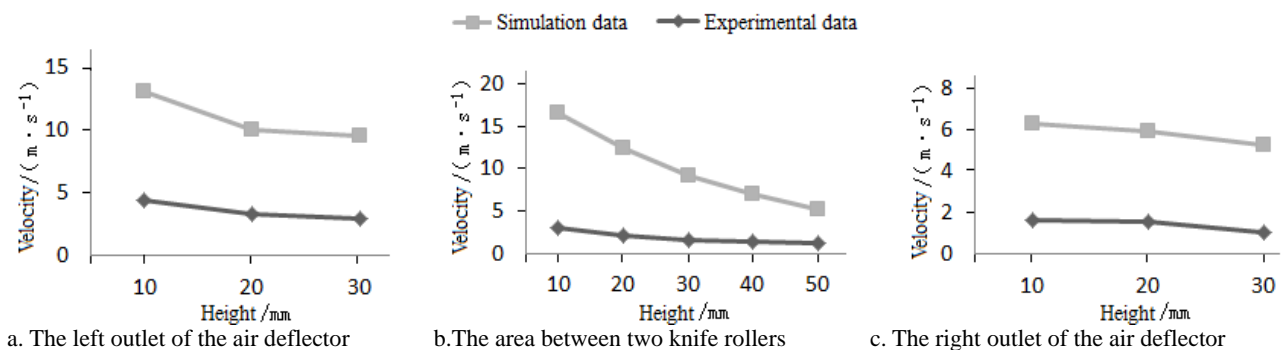
Fig.8 Comparison of horizontal wind velocity between the simulation data and experiment

Comparison of vertical wind velocities by measurement and simulation are shown in Fig.9. Both of the experimental and simulation data indicate that the vertical wind velocity increases with the increase of height. In general, the vertical wind velocity at the right outlet of the air deflector is higher than that at the left outlet, and it is the lowest in the region between two knife rollers. Again, comparison of the vertical velocity increasing rates obtained by simulation and experiments shows a consistency. Over an elevation increase from 0.01 to 0.03 m above the ground, the simulated and experimental increasing rates of vertical wind velocity are 77% and 51% for the left deflector outlet, 43% and 60% in the region between two knife rollers (where an elevation difference over 0.01 and 0.05 m was considered), and 80% and 91% for the right deflector outlet, respectively. The maximum deviation of increasing rate between the simulated and experimentally measured vertical wind velocity is 26%, i.e. the increasing trend of the simulated vertical wind velocity agrees well with the experimental results.

a. The left outlet of the air deflector   b.The area between two knife rollers   c. Theright outlet of the air deflector
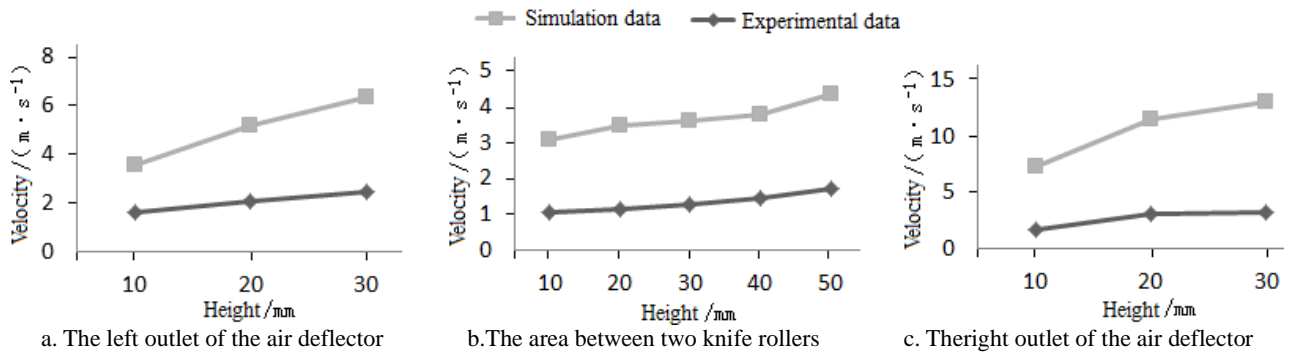
Fig.9 Comparison of vertical wind velocity between the simulation data and experiment

Fig.8 and Fig.9 indicate that our simulation and experimental data gives a consistent relationship between wind velocity variations and heights in different regions near the ground. There is a deviation of simulation data compared with the experimental values, which can be resulted from the unoptimized parameter setting of the simulation model, model simplification, measurement error of the anemometer, and so on.

6. Conclusions

（1） Simulation results show an airflow confluence surface generated in the region between two knife rollers, accompanied by formation of one or two vortices near the confluence surface. Airflow is regular and stable in the left and right outlets of the air deflector and the region near the ground between two knife rollers. Contrarily, airstreams in the middle regions of the air deflector is fluctuating due to the presence of vortices.

（2） The wind velocity changes periodically with a frequency within the range of 50 to 100 Hz. The horizontal wind velocity is the highest in the left outlet of the air deflector, while the maximum vertical wind velocity is in the right outlet of the air deflector.

（3） Both the simulation and experimental data of horizontal wind speed indicate a decreasing trend with the increase of elevation. The maximum deviation of decreasing rates between simulation and experimental data is 12%. The vertical wind velocity is increasing with the increase of elevation. The maximum deviation of increasing rates between simulation and experimental data is 26%. The trend of velocity variations revealed by simulation and experimental data is consistent. Insights from this study can be useful in designing and optimizing relevant air guiding and air-elastomer interaction structures.

Acknowledgements

References

[1]. Wang Liuyi，Lv Youjie，TANG Yanqin，et al. Design and research of the remote-controlled machine for cutting off Sugarcane leaf[J].Journal of Agricultural Mechanization Research，2006(9):93-95.

[2]. Wang Jing. Design and Research of Sugarcane Leaf Cutting off Returning to Field Machinery[D].Guangzhou：South China Agricultural University，2014.

[3]. Jing Wang，Yuxing Wang，Yanqin Tang，et al. Finite element analysis of the chassis for sugarcane leaf cutting off returning to field machinery [J]. Advanced Materials Research，2014，915-916：305-309.

[4]. Tutt B A，Taylor A P. The use of LS-DYNA to simulate the inflation of a parachute

canopy[R].AIAA 2005-1608，2005.

[5]. Tutt B A，Taylor A P，Jean C B，et al. The use of LS-DYNA to assess the performance of airborne system North America candidate ATPS main parachutes[R].AIAA 2005-1609，2005

[6]. Tutt B A. The application of a new material porosity algorithm for parachute analysis[C]. The 9th International LS-DYNA Users Conference，2006.

[7]. Lingard J S，Darley M G. Simulation of parachute fluid structure interaction in supersonic flow[R].AIAA 2005-1607，2005.

[8]. Lingard J S，Darley M G，Underwood J C. Simulation of mars supersonic parachute performance and dynamics[R]. AIAA 2007-2507，2007.

[9]. Jia He，Rong Wei，Chen Guoliang. The use of LS- DYNA to simulate the permeability parameters of the parachute canopy [J]. Spacecraft Recovery & Remote Sensing，2009，30(1)：15-20.

[10]. Jia He，Rong Wei，Chen Guoliang，et al. The simulation of parachute inflation process based on LS-DYNA software [J]. Spacecraft   Environment   Engineering，2010，27(3): 367-373.

[11]. Chen Han，Yu Li，Li Shaoteng，et al. A study on the opening process of folded parachute[J]. Spacecraft Recovery & Remote Sensing.2012，33(2)：1-6.

[12]. Chen Han，Yu Li，Li Shengquan. Numerical simulation of parachute inflation process based on ALE[J]. Journal of Nanjing University of Aeronautics& Astronautics，2012，44(3)：290-293.

[13]. Taylor A P. Developments in the application of LS-DYNA to fluid structure interaction (FSI) problems in recovery system design and analysis [C].   The 7th International LS-DYNA Users Conference, Fluid /Structure. Michigan: LSTC & ETA, 2002: 10-17.

[14]. Tutt B A，Taylor A P. The use of LS-DYNA to simulate the water landing characteristics of space vehicles [C]. The 8th International LS-DYNA Users Conference, Fluid / Structure Michigan：LSTC& ETA，2004：1-15.

[15]. Ma Chunsheng，Huang Shilin，Zhang Jinhuan，et al. Simulations of the landing of manned spacecraft with parachutes using the ALE method in LS-DYNA[J].Journal of Tsinghua University Science and Technology，2006，46(8)：1455-1457.

[16]. Zhang Xuhuai，Du Huiliang，Ma Chunsheng，et al. Water impact simulations and analyses of space capsule response characteristics [J]. Journal of Tsinghua University Science and Technology，2010，50(8)：1297-1301.

[17]. Cheng Zaibin，Liu Yubiao，Liu Zhao，et al. FSI simulation on the vertical launching process of underwater missile [J]. Acta Armamentarii，2008，29(2)：178-183.

[18]. Jiaxian Lu，Yuxing Wang，Yanqin Tang，et al. Fatigue analysis of large-deformation cutting tool used in cutting-off sugarcane-leaf returning machine [J]. Researches and Applications in Mechanical Engineering,，Volume 3，2014: 54-57.

[19]. Yu Hongxuan，Research on Fluid Structure Integration of the Parachute during Opening Processing[D]. Nanjing：Nanjing University of Aeronautics and Astronautics，2010